AFRL-AFOSR-UK-TR-2012-0057

Extension of Flutter Boundaries Using In-Flight Receptance Data

Professor John E Mottershead

University of Liverpool
Centre for Engineering Dynamics
Harrison-Hughes Building
Liverpool, United Kingdom L69 3GH

Report Date: 1 November 2012

Final Report for 15 June 2010 to 14 January 2013

Air Force Research Laboratory
Air Force Office of Scientific Research
European Office of Aerospace Research and Development
Unit 4515 Box 14, APO AE 09421

REPORT DOCUMENTATION PAGE

Form Approved OMB No. 0704-0188

1. REPORT DATE *(DD-MM-YYYY)*	2. REPORT TYPE	3. DATES COVERED *(From – To)*
1 November 2012	Final Report	15 June 2010 – 14 January 2013

4. TITLE AND SUBTITLE

Extension of Flutter Boundaries Using In-Flight Receptance Data

5a. CONTRACT NUMBER

FA8655-10-1-3054

5b. GRANT NUMBER

Grant 10-3054

5c. PROGRAM ELEMENT NUMBER

61102F

6. AUTHOR(S)

Professor John E Mottershead

5d. PROJECT NUMBER

5d. TASK NUMBER

5e. WORK UNIT NUMBER

7. PERFORMING ORGANIZATION NAME(S) AND ADDRESS(ES)

University of Liverpool
Centre for Engineering Dynamics
Harrison-Hughes Building
Liverpool, United Kingdom L69 3GH

8. PERFORMING ORGANIZATION REPORT NUMBER

N/A

9. SPONSORING/MONITORING AGENCY NAME(S) AND ADDRESS(ES)

EOARD
Unit 4515 BOX 14
APO AE 09421

10. SPONSOR/MONITOR'S ACRONYM(S)

AFRL/AFOSR/EOARD

11. SPONSOR/MONITOR'S REPORT NUMBER(S)

AFRL-AFOSR-UK-TR-2012-0057

12. DISTRIBUTION/AVAILABILITY STATEMENT

Approved for public release; distribution is unlimited. (approval given by local Public Affairs Office)

13. SUPPLEMENTARY NOTES

14. ABSTRACT

This report describes an experimental study involving the implementation of the method of receptances to control binary flutter in a wind-tunnel aerofoil rig. The aerofoil and its suspension were designed as part of the project. The advantage of the receptance method over conventional state-space approaches is that it is based entirely on frequency response function measurements, so that there is no need to know or to evaluate the system matrices describing structural mass, aeroelastic and structural damping and aeroelastic and structural stiffness. There is no need for model reduction or the estimation of unmeasured states, for example by the use of an observer. It is demonstrated experimentally that a significant increase in the flutter margin can be achieved by separating the frequencies of the heave and pitch modes. In the test carried out so far it has been found that simply increasing the damping, principally of the heave mode, is less effective in increasing the flutter margin than separating the heave and pitch frequencies.

15. SUBJECT TERMS

EOARD, Structural Dynamics, Flutter Suppression, Aeroelasticity

16. SECURITY CLASSIFICATION OF:			17. LIMITATION OF ABSTRACT	18, NUMBER OF PAGES	19a. NAME OF RESPONSIBLE PERSON
a. REPORT	b. ABSTRACT	c. THIS PAGE			Gregg Abate
UNCLAS	UNCLAS	UNCLAS	SAR	21	19b. TELEPHONE NUMBER *(Include area code)* +44 (0)1895 616021

Extension of Flutter Boundaries Using In-Flight Receptance Data.

FINAL REPORT

1 November 2012

EOARD Contract FA8655-10-1-3054

Prof J.E. Mottershead
Centre for Engineering Dynamics,
University of Liverpool

Prof J.E. Cooper
Department of Aerospace Engineering
University of Bristol

Summary

This report describes an experimental study involving the implementation of the method of receptances to control binary flutter in a wind-tunnel aerofoil rig. The aerofoil and its suspension were designed as part of the project. The advantage of the receptance method over conventional state-space approaches is that it is based entirely on frequency response function measurements, so that there is no need to know or to evaluate the system matrices describing structural mass, aeroelastic and structural damping and aeroelastic and structural stiffness. There is no need for model reduction or the estimation of unmeasured states, for example by the use of an observer. It is demonstrated experimentally that a significant increase in the flutter margin can be achieved by separating the frequencies of the heave and pitch modes. In the test carried out so far it it has been found that simply increasing the damping, principally of the heave mode, is less effective in increasing the flutter margin than separating the heave and pitch frequencies.

Contents

Nomenclature

$\boldsymbol{A}$	Structural mass matrix
$\boldsymbol{b}$	Input distribution vector
$\boldsymbol{B}$	Aerodynamic damping matrix
$\boldsymbol{C}$	Aerodynamic stiffness matrix
$\boldsymbol{D}$	Structural damping matrix
$\boldsymbol{E}$	Structural stiffness matrix
$\boldsymbol{f}, \boldsymbol{g}$	Vectors of control gains
$\boldsymbol{H}(\omega)$	Frequency response function matrix / Receptance matrix
$\boldsymbol{H}(s)$	Transfer function matrix / Receptance matrix
$\boldsymbol{p}$	Vector of control inputs / forces
$\boldsymbol{q}, \dot{\boldsymbol{q}}$	Vectors of state variables / displacements and velocities
s	Laplace variable
v	Air speed
β	Flap angle
ζ_j	j^{th} damping ratio
λ_j	j^{th} open loop eigenvalue
μ_j	j^{th} closed loop eigenvalue
ω_j	j^{th} natural frequency

1. Introduction.

Aeroservoelasticity (ASE) is the engineering science of structural deformation interacting with aerodynamic and control forces [1-2]. It is an essential component for the design of next-generation flexible and maneuverable aircraft and sensorcraft, manned or unmanned, as well as for new flight control systems (FCS). One of the goals of ASE is to overcome the dynamic instability phenomenon of *flutter*, which can lead to catastrophic structural failure when the aircraft structure starts to absorb energy from the surrounding aerodynamic flow [3-5]. The suppression of flutter, achieved by either passive or active means [6-8], may be considered as an inverse eigenvalue problem [9], often referred to as eigenvalue assignment. Passive techniques for flutter suppression may require mass balancing and structural stiffness or shape modifications. Although such passive techniques are considered very robust in their performance, they introduce additional weight and possibly constraints that may be prohibitive to aircraft performance. Alternatively, by supplying active control

forces using sensors and actuators embedded in the aircraft structure, the desired performance may be achieved actively. For example, forces originating from the coupling of the structure with the aerodynamic flow may be modified and flutter suppressed by actively controlling the ailerons or reshaping the surface of wings (morphing) to optimize a performance objective.

For an adequately designed aircraft, flutter will occur outside the desired flight envelope, at some matched dynamic pressure and Mach number. Both military and commercial aircraft designs require a 15% flutter free margin beyond the designed speed and altitude envelope [3]. In order to develop the next-generation aircraft or spacecraft, or to improve the performance of existing aircraft, the extension of flutter-free margins needs to be realized by active suppression techniques using existing control surfaces. However, it should be noted that no aircraft is currently flown beyond its flutter speed through the incorporation of a flutter suppression system.

The main objective of this study is to demonstrate in principle that by using on-board sensor and control surfaces, the flutter boundaries of a given flight envelope can be extended using active control techniques based upon vibration measurements. In recent years, the theory and application of pole placement by the receptance method have been developed in a series of papers [10]-[14] based upon this idea. The main idea of the receptance method is to obtain and utilize transfer function data from available sensors and actuators, and to design control gains purely based upon such measurements. The receptance approach has a number of significant advantages over conventional pole-placement methods, either cast in the first-order state-space or as second-order matrix polynomials [15]. There is no need to know or to evaluate the structural matrices that usually contain various modelling assumptions and errors, and must be brought into agreement with test data by model updating.

A further approximation for aeroelastic systems is that the unsteady aerodynamic forces must also be modelled, typically using a frequency domain analysis. For ASE applications, it is usual to approximate the frequency domain aerodynamics, extracted from the aeroelastic influence coefficient (AIC) matrix at a set of discrete frequencies [3,16] into the time domain, via a rational fraction approximation of the aerodynamics. This procedure, generally dependent upon finite element codes such as MSC-NASTRAN, ZAERO or ASTROS, is rendered completely unnecessary by the receptance method which captures the coupled aeroelastic behaviour in the measurement. The word *receptance* comes from the first theoretical papers which assumed force inputs and displacement outputs, but is now a misnomer, since the inputs and outputs may be any measurable quantities. This means that the measured inputs and outputs may, for example, be input and output voltage signals to the actuators and from the sensors, so that the sensor and actuator dynamics are included in the measured data. The sensors and actuators do not have to be collocated. There is no requirement to estimate unmeasured state variables by an observer or Kalman filter, and no need for model reduction. This may be understood by consideration of the system equations, in receptance form they are displacement equations, whereas by conventional methods force equations are formed using dynamic stiffnesses. It is seen that a complete displacement equation is formed for each measured degree of freedom provided each of the external forces applied by a small number of actuators is measured. Conversely the force equations are not complete unless all the degrees of freedom are measured; this requires estimation of the unmeasured state variables.

For ASE control application, the available matrix of receptances is usually quite modest in size, determined entirely by the number of available on-board sensors and actuators. For example, in order to compute the receptance transfer function, the input might be the voltage applied to a motor for movement of a control surface, and the output may be obtained from embedded accelerometers. The number of sensors is generally equal to the number of eigenvalues to be assigned, provided that the eigenvalues are observable. In principle a single actuator can assign all the eigenvalues, which must be simple and controllable, and may be implemented using time-varying control requiring the in-flight measurement of receptances and determination of control gains.

This report describes the theory of the method of receptances and its implementation on a wind-tunnel aerofoil rig, which was designed and constructed as part of this project. The receptance method is implemented by fitting rational fraction polynomials to measured frequency response functions (FRFs), in the present case the inputs are the voltages applied to a power amplifier supplying a 'V' stack piezo-actuator and the outputs are laser sensor displacement signals (and velocities obtained by numerical differentiation in dSPACE[1]). The measured FRFs include not only the dynamics of the system but also of the actuator and sensors and the effects of A/D and D/A conversion, numerical differentiation and the application of high-pass and low-pass Butterworth filters in dSPACE. Successful pole placement is achieved in preliminary tests and finally flutter-margin extension is demonstrated by two methods: (1) separating the frequencies of the heave and pitch modes and (2) increasing the damping, principally of the heave mode. The first of these two approaches is found to be the most effective.

2. Preliminary Theory

The governing equation of an aeroelastic system can be written as [3]

$$\boldsymbol{A}\ddot{\boldsymbol{q}} + (\rho v\boldsymbol{B} + \boldsymbol{D})\dot{\boldsymbol{q}} + (\rho v^2\boldsymbol{C} + \boldsymbol{E})\boldsymbol{q} = \boldsymbol{p} \tag{1}$$

where, $\boldsymbol{A}, \boldsymbol{B}, \boldsymbol{C}, \boldsymbol{D}, \boldsymbol{E}$ are the structural inertia, aerodynamic damping, aerodynamic stiffness, structural damping and structural stiffness matrices respectively, $\boldsymbol{q}(t)$ is the vector of generalised coordinates, $\boldsymbol{p}(t)$ is the vector of control forces. The aerodynamic forces, for a chosen Mach number and reduced frequency, are expressed as additional contributions to the system matrices. In equation (1) these terms appear as matrices $\boldsymbol{B}$ and $\boldsymbol{C}$ which, in general, are frequency dependent. Often these forces are combined together in the form of the aeroelastic influence coefficient (AIC) matrix at a set of discrete frequencies. Here, a simplified aeroelastic modeling approach will be used that still maintains the key characteristics of unsteady aerodynamic behaviour [3].

For the open-loop homogenous system, using separation of variables $\boldsymbol{q}(t) = \sum_{j=1}^{2n} \alpha_j \boldsymbol{\varphi}_j \exp(\lambda_j t)$, the eigenvalue equation of the j^{th} mode is expressed as

$$\left(\lambda_j^2\boldsymbol{A} + (\rho v\boldsymbol{B} + \boldsymbol{D})\lambda_j + (\rho v^2\boldsymbol{C} + \boldsymbol{E})\right)\boldsymbol{\varphi}_j = \boldsymbol{0} \tag{2}$$

[1] http://www.dspace.com/en/inc/home.cfm

Where α_j is the j^{th} modal coordinate. The complex eigenvalues in equation (2) may be written in terms of the j^{th} damping and natural frequency, which are determined from the real and imaginary parts of the characteristic eigenvalues (or poles). For the models used in this report, the matrices, $\boldsymbol{A}, \boldsymbol{B}, \boldsymbol{C}, \boldsymbol{D}, \boldsymbol{E}$, are strictly real and constant, with the eigenvalues (and eigenvectors) appearing in complex conjugate pairs such that

$$\lambda_{j,n+j} = -\zeta_j \omega_j \pm \mathrm{i}\omega_j \sqrt{\left(1-\zeta_j^2\right)} \qquad j = 1, 2, \ldots, n \tag{3}$$

For more accurate models, the aerodynamic matrices $\boldsymbol{B}$ and $\boldsymbol{C}$ are complex and depend upon the reduced frequency. This approximation does not affect the accuracy of the control approach, which is the main focus of this work.

The real part of the eigenvalues defines the stability of the system and, when the real part of the eigenvalues λ_j in equation (3) is positive, the system is unstable and results in flutter. The system considered here has linear structural and aerodynamic models, so non-linear phenomena such as Limit Cycle Oscillations (LCOs) cannot occur. For all other values of the real part of the eigenvalues, the aeroelastic system is either stable or marginally stable.

Flutter of the aircraft, or its components, is a dynamic instability associated with the aeroelastic system which involves interaction and coupling of modes (wing bending/torsion, wing torsion/control surface, wing/engine, etc.) that results in energy being extracted from the airstream leading to negatively damped modes and unstable oscillations. For a given Mach number, at some critical speed (flutter speed) the eigenvalues exhibit instability, leading to sustained oscillations which can result in catastrophic failure. In a flutter analysis the eigenvalues, and hence the natural frequencies and damping ratios, are computed for varying speeds, altitudes and Mach numbers, and the critical flutter speeds determined. In aeroelastic control, the goal is to suppress flutter, or extend the flutter boundaries, by assigning stable poles using feedback control forces, usually supplied by available control surfaces e.g. ailerons.

The system matrices in equations (1) and (2) depend upon the aeroelastic system, the number of degrees of freedom, and on the position and size of the control surfaces. The objective of the approach is to use the Receptance Control Method in order to define the control forces required to place the closed loop poles in such a manner that the onset of flutter is delayed. This is achieved by placing the closed loop poles at different, more advantageous, positions in the complex plane compared to those of the open loop system.

3. Active Control by the Method of Receptances

The approach used in this work will be demonstrated using a binary aeroelastic system, shown in Figure 1, which incorporates a control surface as part of a closed loop feedback system. Note that the control surface is not a flexible degree of freedom, but provides a means to impart a force onto the aerofoil which is proportional to the control angle β.

The receptance matrix of the open loop system may be expressed in the complex Laplace domain as the inverse of the aeroelastic dynamic stiffness matrix,

$$\boldsymbol{H}(s) = \left(\boldsymbol{A}s^2 + (\rho v \boldsymbol{B} + \boldsymbol{D})s + (\rho v^2 \boldsymbol{C} + \boldsymbol{E})\right)^{-1} \tag{4}$$

However, in practice it is determined from frequency response functions (FRFs) estimated from power and cross spectral densities of force and response measurements using well known procedures, for example described by Bendat and Piersol [17]. Curve fitting of the estimated $\boldsymbol{H}(\mathrm{i}\omega)$, for example by the PolyMAX routine [18], allows the determination of $\boldsymbol{H}(s)$ by substituting *s* for $\mathrm{i}\omega$ in the curve-fitted approximation; this approach was demonstrated in active vibration control by Tehrani *et al.* [19]. In this paper we assume that the matrix of receptances can be determined from in-flight measurements of aeroelastic inputs and outputs. It can be demonstrated [19] that any input and output signals may be used in aeroelastic eigenvalue assignment, in which case the dynamics of actuators and sensors (including the effects of time delay) may be included in the measurement, rendering unnecessary the need for mathematical models to approximate the behavior of actuators and sensors.

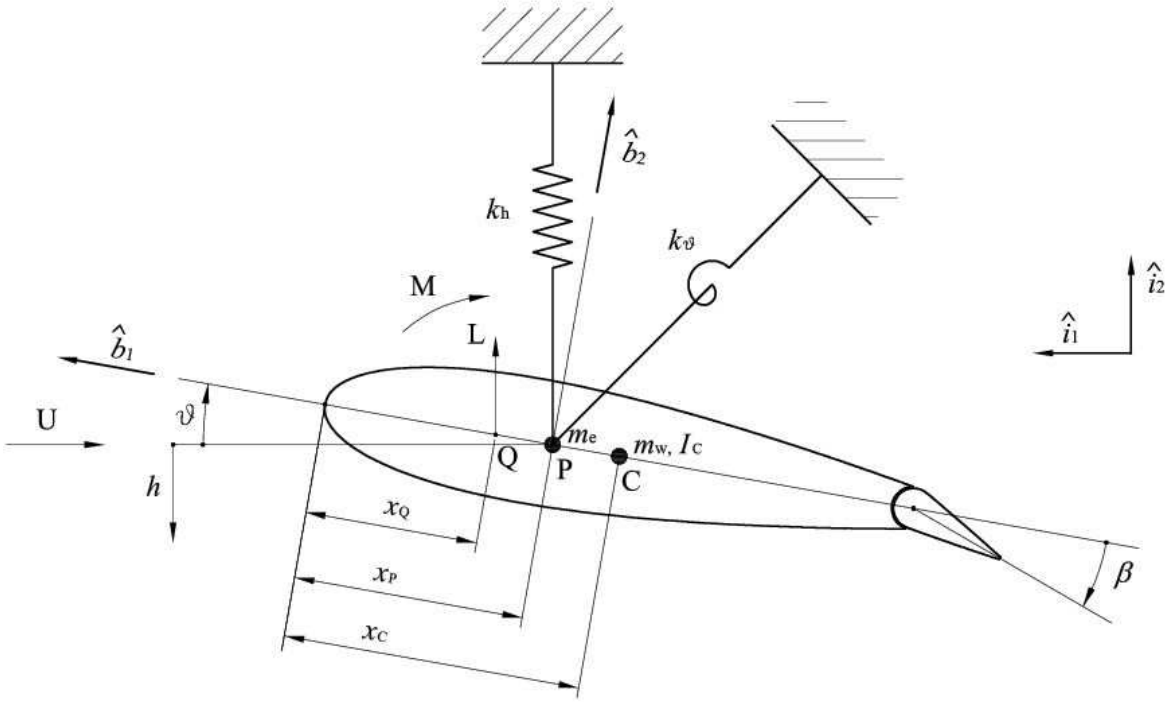

Figure 1: Binary Airfoil Configuration with Control Surface.

The method depends upon a very useful result from the linear algebra, namely the Sherman-Morrison formula, which produces a modified inverse matrix, $\overline{\boldsymbol{Z}}^{-1} = (\boldsymbol{Z} + \boldsymbol{u}\boldsymbol{v}^T)^{-1}$, when a known rank 1 modification, $\boldsymbol{u}\boldsymbol{v}^T$, and original inverse matrix, $\boldsymbol{Z}^{-1}$, are available such that

$$\overline{\boldsymbol{Z}}^{-1}(s) = \boldsymbol{Z}^{-1}(s) - \frac{\boldsymbol{Z}^{-1}(s)\boldsymbol{u}(s)\boldsymbol{v}^T(s)\boldsymbol{Z}^{-1}(s)}{1+\boldsymbol{v}^T(s)\boldsymbol{Z}^{-1}(s)\boldsymbol{u}(s)} \tag{5}$$

In single-input control, the control force is typically given by

$$\boldsymbol{p}(t) = \boldsymbol{b}u(t) \tag{6}$$

where

$$u(t) = \boldsymbol{f}^t \dot{\boldsymbol{q}} + \boldsymbol{g}^T \boldsymbol{q} \tag{7}$$

for displacement and velocity feedback, where the gains $\boldsymbol{f}$ and $\boldsymbol{g}$ are such that the closed loop system has new (closed-loop) complex poles $\mu_{j,n+j}$, $j = 1, \dots, n$.

By combining equations (1), (6) and (7), we get

$$\boldsymbol{A}\ddot{\boldsymbol{q}} + (\rho v \boldsymbol{B} + \boldsymbol{D} + \boldsymbol{b}\boldsymbol{f}^T)\dot{\boldsymbol{q}} + (\rho v^2 \boldsymbol{C} + \boldsymbol{E} + \boldsymbol{b}\boldsymbol{g}^T)\boldsymbol{q} = \boldsymbol{0} \tag{8}$$

or in the complex Laplace domain

$$\left(\boldsymbol{A}s^2 + (\rho v \boldsymbol{B} + \boldsymbol{D} + \boldsymbol{b}\boldsymbol{f}^T)s + (\rho v^2 \boldsymbol{C} + \boldsymbol{E} + \boldsymbol{b}\boldsymbol{g}^T)\right)\boldsymbol{q}(\boldsymbol{s}) = \boldsymbol{0} \tag{9}$$

and so the closed-loop eigenvalue equation becomes

$$\left(\boldsymbol{A}\mu_j^2 + (\rho v \boldsymbol{B} + \boldsymbol{D} + \boldsymbol{b}\boldsymbol{f}^T)\mu_j + (\rho v^2 \boldsymbol{C} + \boldsymbol{E} + \boldsymbol{b}\boldsymbol{g}^T)\right)\boldsymbol{\psi}_j = \boldsymbol{0} \tag{10}$$

Where μ_j, $\boldsymbol{\psi}_j$, μ_{n+j}, $\boldsymbol{\psi}_{n+j}$, $j = 1, \dots, n$ denote the closed-loop eigenvalues and eigenvectors in complex-conjugate pairs.

Evidently, from equation (9), the open-loop system is changed by the rank 1 modification, $\boldsymbol{b}(s\boldsymbol{f} + \boldsymbol{g})^T$. Therefore, the closed-loop receptance matrix is given from the Sherman-Morrison formula as

$$\bar{\boldsymbol{H}}(s) = \boldsymbol{H}(s) - \frac{\boldsymbol{H}(s)\boldsymbol{b}(s\boldsymbol{f}+\boldsymbol{g})^T\boldsymbol{H}(s)}{1+(s\boldsymbol{f}+\boldsymbol{g})^T\boldsymbol{H}(s)\boldsymbol{b}} \tag{11}$$

and, from the denominator of equation (11), the control gains f, g must be chosen so that the equations

$$\left.\begin{matrix} 1 + \left(\mu_j \boldsymbol{f} + \boldsymbol{g}\right)^T \boldsymbol{H}(\mu_j)\boldsymbol{b} = \boldsymbol{0} \\ 1 + \left(\mu_{n+j} \boldsymbol{f} + \boldsymbol{g}\right)^T \boldsymbol{H}(\mu_{n+j})\boldsymbol{b} = \boldsymbol{0} \end{matrix}\right\} \quad j = 1, \dots, n \tag{12}$$

are satisfied for the assignment of the closed-loop eigenvalues in complex-conjugate pairs $\mu_{n+j} = \mu_j^\star$.

Re-arranging and combining equations (12) into a single matrix expression leads to

$$\boldsymbol{G}\begin{pmatrix}\boldsymbol{g}\\ \boldsymbol{f}\end{pmatrix} = \begin{pmatrix}-1\\ \vdots \\ -1\end{pmatrix} \tag{13}$$

with

$$\boldsymbol{G} = \begin{bmatrix} \boldsymbol{r}_1^T & \mu_1 \boldsymbol{r}_1^T \\ \boldsymbol{r}_2^T & \mu_2 \boldsymbol{r}_2^T \\ \vdots & \vdots \\ \boldsymbol{r}_{2n}^T & \mu_{2n} \boldsymbol{r}_{2n}^T \end{bmatrix} \tag{14}$$

where

$$\left.\begin{aligned} \boldsymbol{r}_j(\mu_j) &= \boldsymbol{H}(\mu_j)\boldsymbol{b} \\ \boldsymbol{r}_{n+j}(\mu_{n+j}) &= \boldsymbol{H}(\mu_{n+j})\boldsymbol{b} \end{aligned}\right\} \tag{15}$$

which allows the determination of f and g by inversion of the matrix G. Ram and Mottershead [10] showed that

I. $\boldsymbol{G}$ is invertible when the system is controllable and the poles μ_j , $j = 1,2,\ldots 2n$ are distinct, and
II. $\boldsymbol{f}$ and $\boldsymbol{g}$ are real when $\boldsymbol{G}$ is invertible and the set μ_j , $j = 1,2,\ldots 2n$ are closed under conjugation [9].

When $\boldsymbol{G}$ is a square matrix there is a unique solution for $(\boldsymbol{g} \quad \boldsymbol{f})^T$ and when the system (14) is under-determined (fewer poles to be assigned than the number of gain terms, $\boldsymbol{f}$, $\boldsymbol{g}$) then a minimum norm solution is available for the minimization of control effort. Alternatively, in the latter case, the gains may be chosen that assign the chosen eigenvalues while at the same time minimizing the sensitivity of the assigned poles to inaccuracy and noise in the measured receptances. A robust pole-placement approach to noise on the measured receptances is described by Tehrani et al. [14].

4. The Experimental Rig

The wind tunnel experiment consists of a working section containing a NACA0018 aerofoil (chord = 0.35 m, span = 1.2m), supported by adjustable vertical and torsional leaf springs. The aerofoil can be modelled as a 2D system with pitch and plunge degrees of freedom as illustrated in Figure 1.

The design allows the adjustment of the stiffnesses of the vertical and torsional springs, k_h and k_ϑ. The maximum air speed for the wind tunnel used is around 20 m/s. The aim of the design is to explore regions close to the flutter speed of the system.

The vertical spring arrangement is shown in Figure 2. By varying the clamp location in the direction shown in the figure, it is possible to vary the stiffness of the vertical springs, one on each side of the wind tunnel, which support the wing (attached to the shaft on the left of the figure). The vertical stiffness is variable in the range 200 to 23000 N/m.

The adjustable torsional spring is shown in Figure 3. By moving the device in the direction indicated by the arrows it is possible to increase or reduce the torsional stiffness in the range 10 to 320 Nm/rad.

Using these ranges of stiffness, it is possible to vary the flutter speed of the aeroelastic system approximately between 10 and 70 m/s. The open working section (with sides removed and separated from the wind tunnel) is shown in Figure 4(b). A torsional bar is used in order to maintain the same vertical displacement on the two sides of the test section. The external mass of the system was calculated to be around 6.5 Kg.

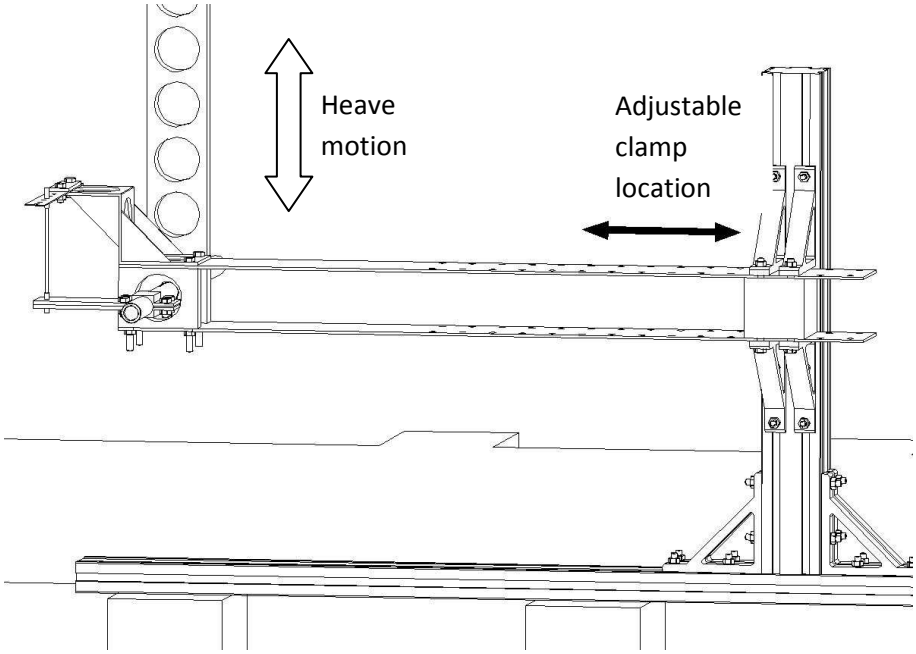

Figure 2: Adjustable Vertical Spring

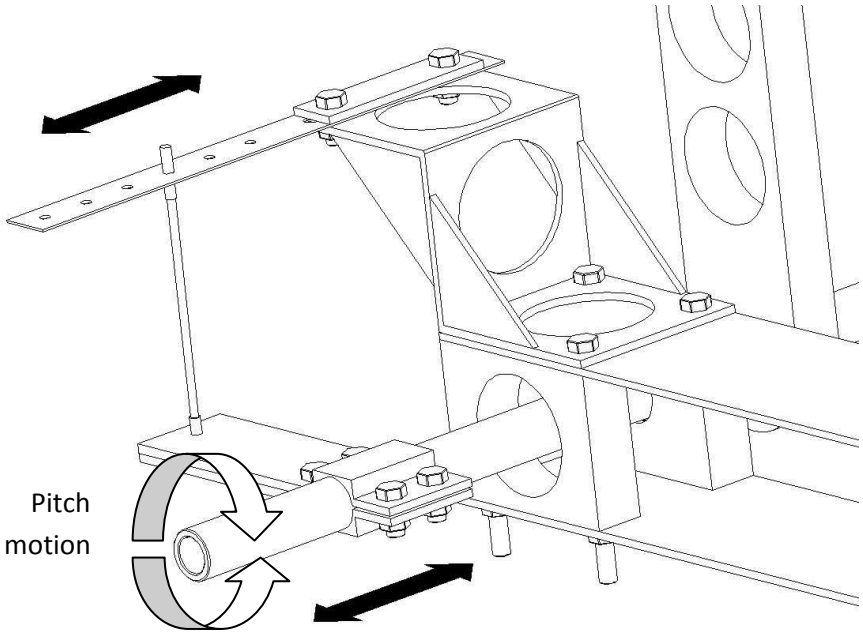

Figure 3: Adjustable Torsion Spring

Active vibration control described in [20, 21] is achieved by means of a 'V'-stack piezoelectric actuator shown in Figure 4(a) acting on the control surface of the wing, allowing a flap deflection of about ±7°. The actuator consists of two piezo-stacks (Noliac SCMAP09-H80-A01) in a 'V' formation.

The flap is actuated when one arm of the 'V' is made to extend while the other retracts by an equal amount – caused by applying equal voltages to the two piezo stacks but with 180° phase difference. Khron Hite wideband power amplifiers, model 7500, were used. The 'V' stack actuator [21] is known to behave as a pure gain provided that its natural frequency is well above the frequencies of the assigned poles.

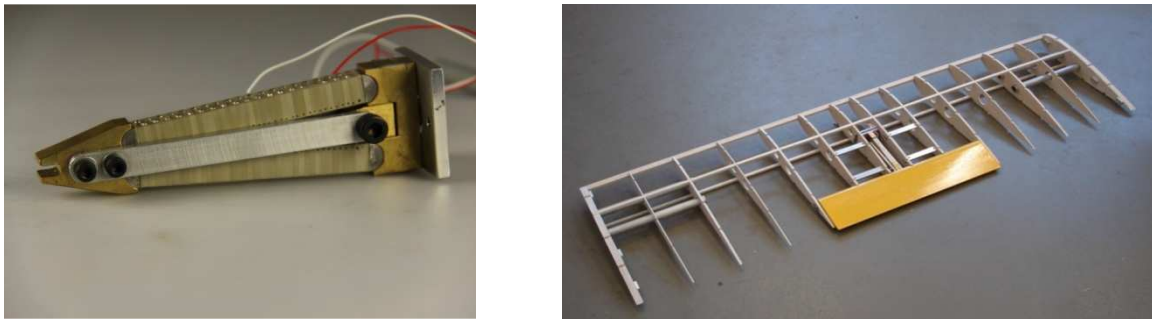

(a) **(b)**

Figure 4: (a) 'V' Stack Actuator; (b) Actuator In-Situ

The receptance method was applied with voltage input to the power amplifiers and displacement output, measured using two laser sensors KEYENCE LK-500 and LK-501. The laser sensors were mounted externally to the working section above a rigid horizontal bar attached to the aerofoil shaft. Separation of the sensors allowed the measurement of both vertical translation and rotation of the shaft (heave and pitch).

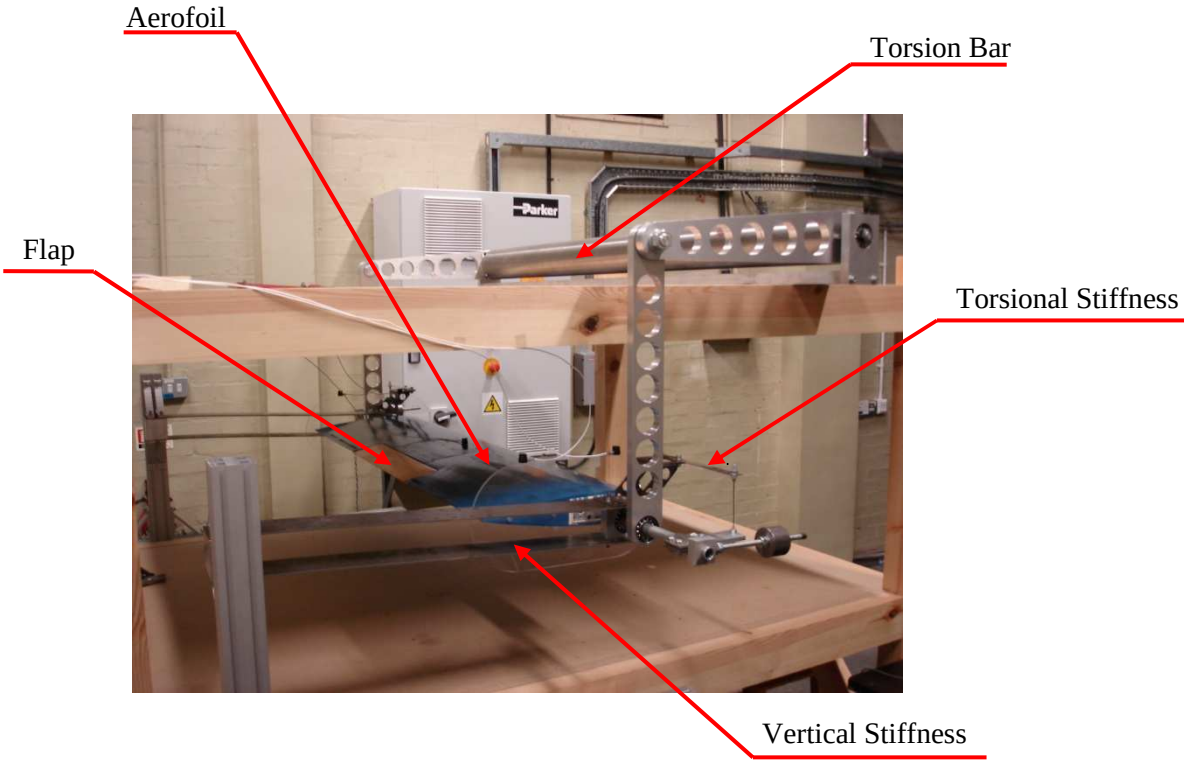

Figure 5: Open Working Section

5. Implementation of the Receptance Method

Frequency response functions (FRFs) relating the power amplifier input voltage v_β to the displacements x_1 and x_2 measured using the laser sensors were determined by stepped-sine testing using a SCADAS III LMS data acquisition system. The frequency range used was 0.5 to 30 Hz and the frequency resolution was 0.05 Hz.

Thus at a chosen wind speed v, the matrix $\boldsymbol{H}(\omega, v)$ in the theory of Section 4 above is given by the relationship,

$$\begin{bmatrix} h_{1,\beta} \\ h_{2,\beta} \end{bmatrix} v_\beta = \begin{pmatrix} x_1 \\ x_2 \end{pmatrix}; \qquad \boldsymbol{H}(\omega, v) = \begin{bmatrix} h_{1,\beta}(\omega, v) \\ h_{2,\beta}(\omega, v) \end{bmatrix} \tag{16}$$

where x_1 and x_2 are the measured displacements. The velocities $\dot{x}_1$ and $\dot{x}_2$ were calculated numerically using Simulink/dSPACE with a sampling rate of 10 kHz and a separate FRF $\dot{\boldsymbol{H}}(\omega, v)$ was determined as,

$$\begin{bmatrix} \dot{h}_{1,\beta} \\ \dot{h}_{2,\beta} \end{bmatrix} v_\beta = \begin{pmatrix} \dot{x}_1 \\ \dot{x}_2 \end{pmatrix}; \qquad \dot{\boldsymbol{H}}(\omega, v) = \begin{bmatrix} \dot{h}_{1,\beta}(\omega, v) \\ \dot{h}_{2,\beta}(\omega, v) \end{bmatrix} \tag{17}$$

The over-dot simply denotes that the FRF relates to the velocity and does not imply differentiation of $\boldsymbol{H}(\omega, v)$.

The open loop FRFs $\boldsymbol{H}(\omega, v)$ and $\dot{\boldsymbol{H}}(\omega, v)$ included not only the dynamics of the aerofoil system but also of the power amplifier, the actuator, the sensors and the effects of A/D and D/A conversion, numerical differentiation of the measured displacements and high-pass and low-pass Butterworth filters with cut-off frequencies of of 1 Hz and 35 Hz respectively (also implemented in dSPACE).

Transfer functions $\boldsymbol{H}(s, v)$ and $\dot{\boldsymbol{H}}(s, v)$ may then be obtained by fitting rational fraction polynomials to the measured $\boldsymbol{H}(\omega, v)$ and $\dot{\boldsymbol{H}}(\omega, v)$. This was achieved using the pole-residue model in the Structural Dynamics Toolbox (SDTools[2]).

Finally, the assignment of two pairs of complex-conjugate poles was achieved by the application of equation (13) with the matrix $\boldsymbol{G}$ given by,

$$\boldsymbol{G} = \begin{bmatrix} \boldsymbol{H}(\mu_1, v) & \dot{\boldsymbol{H}}(\mu_1, v) \\ \boldsymbol{H}(\mu_1^*, v) & \dot{\boldsymbol{H}}(\mu_1^*, v) \\ \vdots & \vdots \\ \boldsymbol{H}(\mu_2^*, v) & \dot{\boldsymbol{H}}(\mu_2^*, v) \end{bmatrix} \tag{18}$$

and $b = 1$ since there is a single actuator and may take an arbitrary value.

It should be noted that at no stage in this process is it necessary to know or to evaluate the matrices $\boldsymbol{A}, \boldsymbol{B}, \boldsymbol{C}, \boldsymbol{D}, \boldsymbol{E}$. Any assumption or mis-modelling of the structural- or aero-dynamics is not included and the performance of the resulting controller depends only upon the quality of the measured frequency response functions $\boldsymbol{H}(\omega, v)$ and $\dot{\boldsymbol{H}}(\omega, v)$.

[2] http://www.sdtools.com/

6. Preliminary Tests - Measurement of FRFs and Pole Placement

One objective of the design of the experimental rig was that the flexible modes of the aerofoil should be well separated from the sprung modes of the aerofoil system, in which the aerofoil is effectively rigid. It is these sprung modes, in pitch and heave, that are to be controlled. A preliminary modal test carried out with a small impact hammer revealed the first bending mode at 41 Hz and first torsion mode of the aerofoil at 47 Hz. There was a mode of the aerofoil support structure (the springs, linkages and torsion bar) at just over 20 Hz and it was important before implementing the controller to ensure that these modes will not be destabilized.

From equations (13) and (18), it is seen that the Nyquist stability criterion is satisfied when $\boldsymbol{H}^T(\omega, v)\boldsymbol{g} + \dot{\boldsymbol{H}}^T(\omega, v)\boldsymbol{f} = [h_{1,\beta} \quad h_{2,\beta}]\begin{pmatrix} g_1 \\ g_2 \end{pmatrix} + [\dot{h}_{1,\beta} \quad \dot{h}_{2,\beta}]\begin{pmatrix} f_1 \\ f_2 \end{pmatrix}$ does not encircle -1.

An example of curve-fitting to a measured FRF using SDTools is shown in Figure 6 for the case of a pitch mode at 3.9 Hz and a heave mode at 6.7 Hz and a wind speed of 7 m/s.

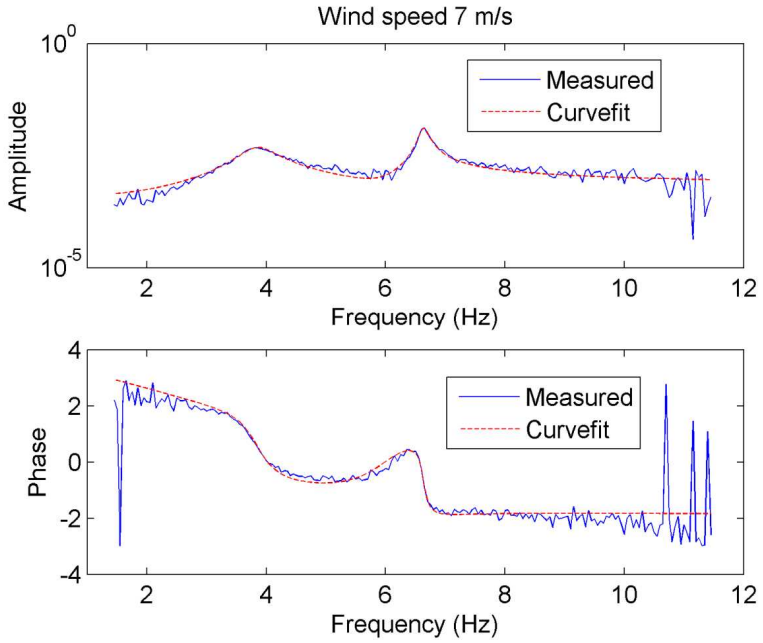

Figure 6. Measured and Curve-Fitted FRFs

An example of pole-placement is given in Figure 7, where (1) the frequency of the heave mode is shifted by a small amount from 6.83 Hz to 7 Hz and an increase of 0.5% damping is assigned and (2) the frequency of the pitch mode is shifted from 3.89 Hz to 3.5 Hz with an increase in damping of 1.5% assigned. The assigned poles are -0.8±44i and -2±22i and the gains are found to be $\boldsymbol{g} = (34.6 \quad 2.45)^T$ and $\boldsymbol{f} = (0.734 \quad 0.427)^T$.

In another example, poles are assigned at -1.5±42.96i and -1.84±24.49i to achieve mainly an increase in damping of the heave mode. The corresponding gains are $\boldsymbol{g} = (-16 \quad -14)^T$ and $\boldsymbol{f} = (0.39 \quad 0.42)^T$. The time-domain response of the aerofoil in open- and closed-loop to an initial

displacement is shown in Figure 8. It is seen that a significant reduction in vibration amplitude is achieved.

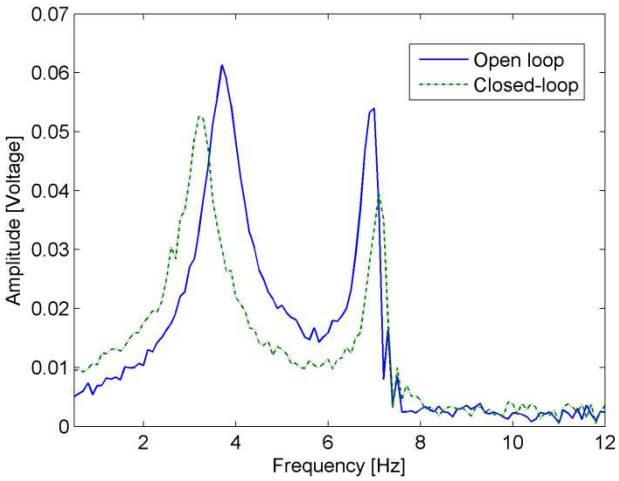

Figure 7. Measured Open- and Closed-Loop FRF after Application of Active Pole Placement

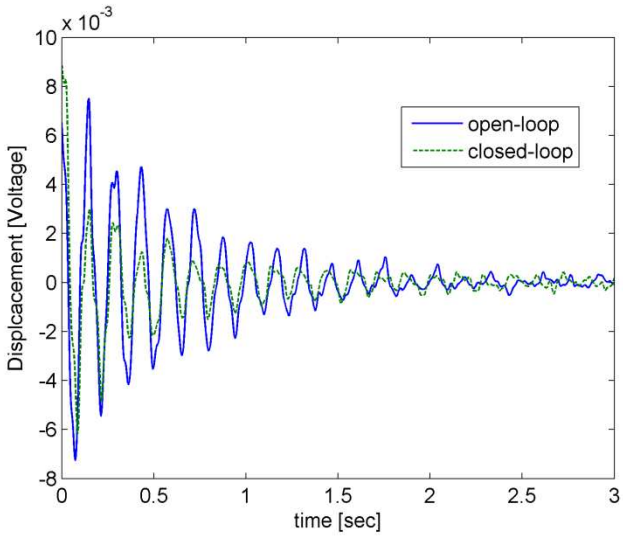

Figure 8. Displacement sensor time-domain response

7. Flutter Margin Control by Pole Placement

The experiments described in this section were carried out with the vertical and torsional srings adjusted to give a heave frequency of approximately 3.6 Hz and a pitch frequency of about 5.6 Hz. Two tests were carried out to achieve an extended flutter margin by (1) separating the heave and pitch frequencies and (2) applying damping principally to the heave mode.

Separating the Heave and Pitch Frequencies

The frequency spacing between the two modes is increased by pole assignment as can be seen in the Figure 9. Pole assignment $\mu_{pitch} = -1.5 \pm 38\text{i}$, $\mu_{heave} = -0.7 \pm 23\text{i}$ is carried out at

$v = 7$ m/s resulting in gains $\boldsymbol{g} = [-28.2 \quad 29.5]^{\mathrm{T}}, \boldsymbol{f} = [0.0284 \quad 0.0232]^{\mathrm{T}}$. The same values of $\boldsymbol{g}$ and $\boldsymbol{f}$ were applied by the controller for air speeds from 6 to 15 m/s.

The Nyquist diagram, shown in Figure 10, is the plot of $[h_{1,\beta} \quad h_{2,\beta}]\begin{pmatrix} g_1 \\ g_2 \end{pmatrix} + [\dot{h}_{1,\beta} \quad \dot{h}_{2,\beta}]\begin{pmatrix} f_1 \\ f_2 \end{pmatrix}$ in the range $0.5 \leq \omega \leq 30$ Hz as explained previously in Section 6. It is seen that for the chosen gains there is a gain margin of 5.2 and a phase margin of 36°, thereby indicating robust stability at $= 7$ m/s .

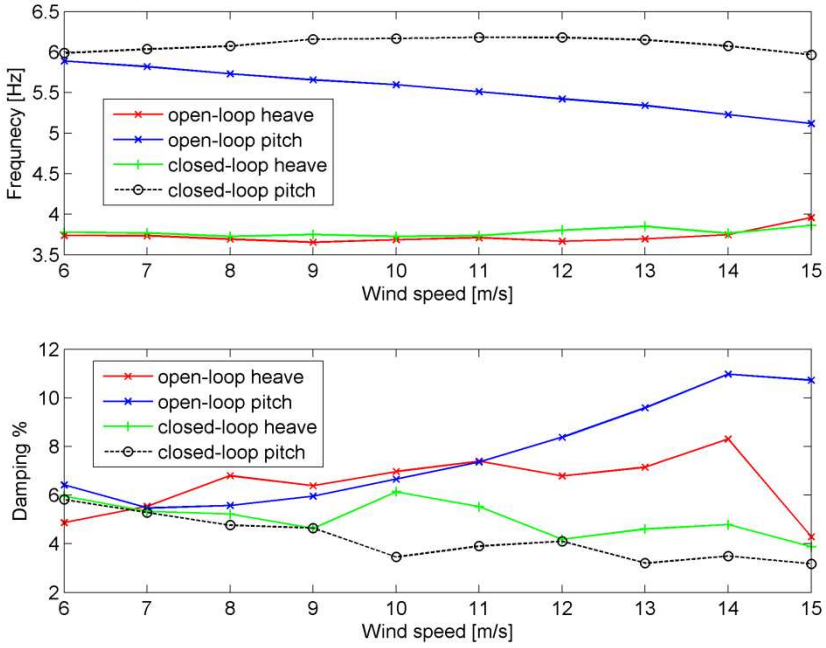

Figure 9. Frequency and Damping of Heave and Pitch Modes with Wind Speed: Open- and Closed-Loop

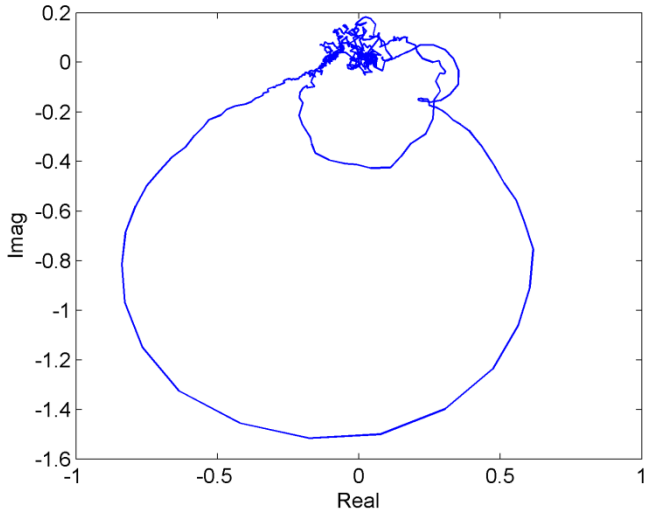

Figure 10. Nyquist Diagram: $v = 7$ m/s, Gain Margin 5.2, Phase Margin 36°

It is seen from Figures 9 that separation of the modal frequencies is achieved mainly by increasing the frequency of the pitch mode, while the heave frequency remains mostly unchanged. The system

was found to undergo quite large control-surface oscillations when an increase in pitch damping as well as in frequency was attempted. In Figures 9 and 11 typical eigenvalue trends leading eventually to flutter may be observed. In Figure 9 the frequency of the closed-loop pitch mode initially increases as v is increased, but after about 12 m/s begins to reduce. Also the damping of the closed-loop pitch mode is consistently less than its open-loop counterpart. The system behaviour becomes very clear in Figure 11 where the locus of the closed-loop pitch mode is seen to be moving towards the imaginary axis and with further increase in air speed will become unstable.

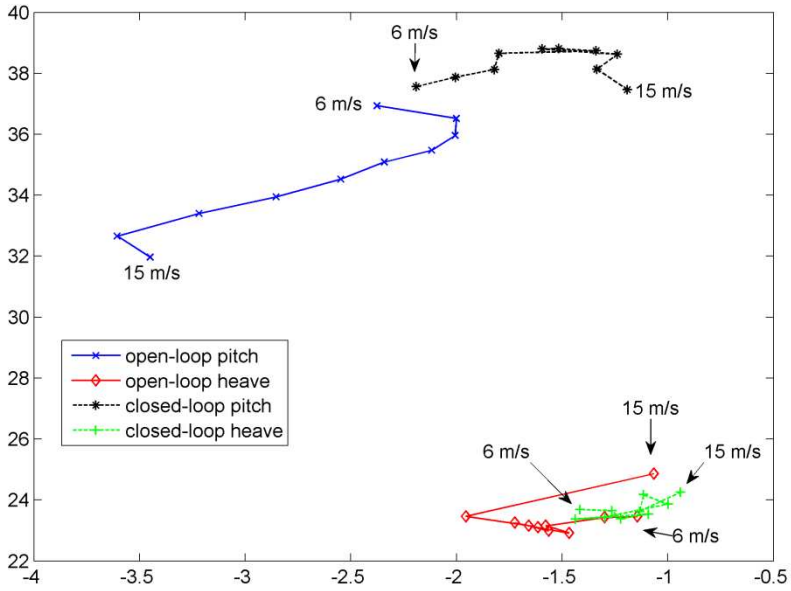

Figure 11. Root Locus with Air Speed.

The flutter margin for a two degree of freedom system (without structural damping) is given by the non-negative function [22-24] of either the open- or closed-loop eigenvalues that satisfies the Routh stability test,

$$F = \left[\left(\frac{\tilde{\omega}_2^2-\tilde{\omega}_1^2}{2}\right)+\left(\frac{\sigma_2^2-\sigma_1^2}{2}\right)\right]^2 + 4\sigma_1\sigma_2\left[\left(\frac{\tilde{\omega}_2^2+\tilde{\omega}_1^2}{2}\right)+2\left(\frac{\sigma_2^2+\sigma_1^2}{2}\right)^2\right] - \left[\left(\frac{\sigma_2-\sigma_1}{\sigma_2+\sigma_1}\right)\left(\frac{\tilde{\omega}_2^2-\tilde{\omega}_1^2}{2}\right)+\left(\frac{\sigma_2+\sigma_1}{2}\right)^2\right]^2 \quad (19)$$

where $\sigma_j = -\zeta_j\omega_j;\ \tilde{\omega}_j = \omega_j\sqrt{(1-\zeta_j^2)};\ j = 1,2.$

It can be shown that the flutter margin, F, is quadratic in the air speed v.

Figure 12 shows two curves obtained by fitting parabolas to experimental values of $F(v)$. The open-loop flutter margin is the full-line blue curve fitted through experimental points given by the red squares. The closed-loop flutter margin is represented by the dashed curve fitted through the experimental black circles. An increase in the flutter speed of around 15% from 17 m/s to 20 m/s is predicted by using the method proposed by Dimitriadis and Cooper [24].

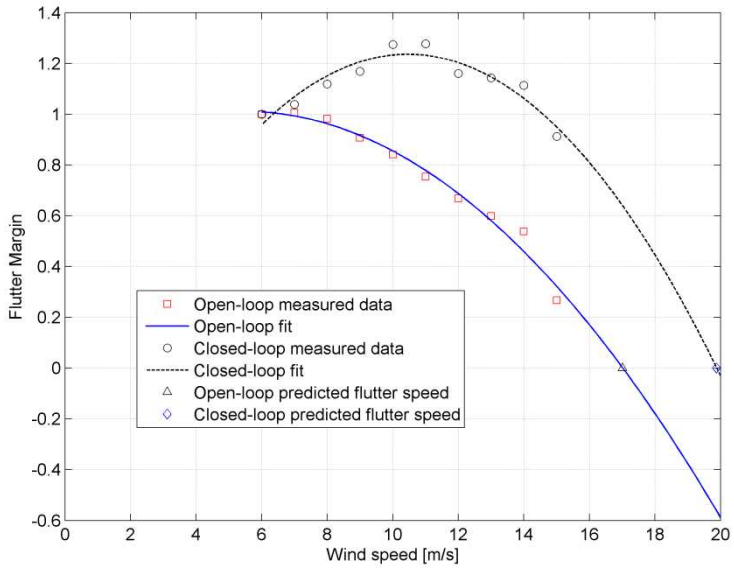

Figure 12. Flutter Margin by Separation of Heave and Pitch Frequencies.

Increasing Damping of the Heave Mode

Poles are assigned as $-1.6 \pm 22\mathrm{i}$ and $-1.7 \pm 37\mathrm{i}$ resulting mainly in an increase in damping of the heave mode at $v = 7\ \mathrm{m/s}$ but also some shifting of the two modes as indicated in Figure 13. The gains, obtained by the receptance method were $\boldsymbol{g} = (-45.3 \quad -2.90)^{\boldsymbol{T}}$ and $\boldsymbol{f} = (-0.0203 \quad 0.02.8)^{\boldsymbol{T}}$. It can be seen from Figure 14 that the flutter speed is increased, but not significantly, from 17 m/s to 17.57m/s.

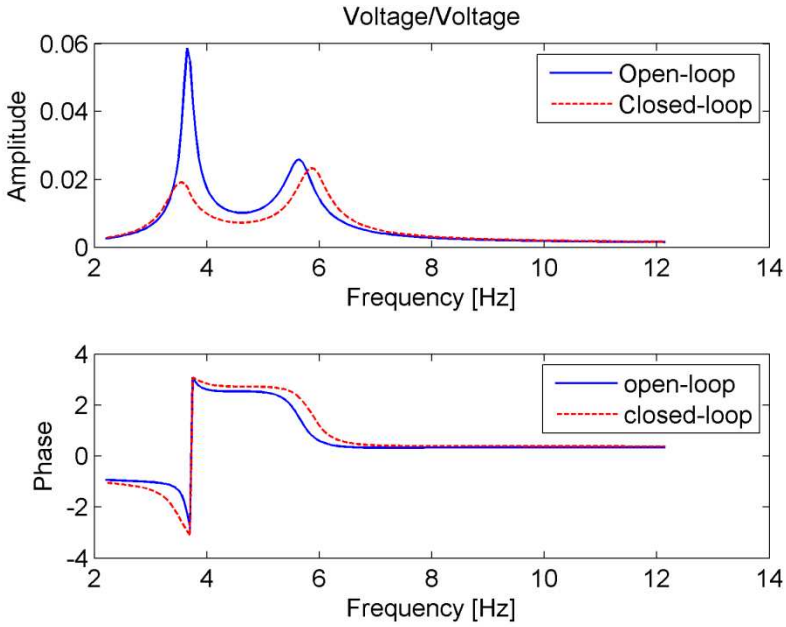

Figure 13. Open- and Closed-Loop FRFs – Increasing Heave Damping

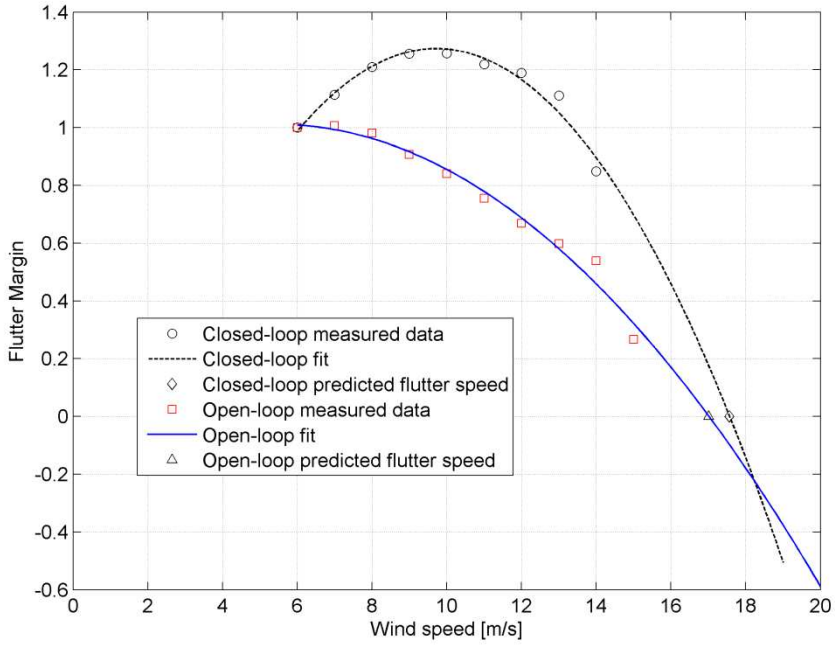

Figure 14. Flutter Margin by Increasing Heave Damping.

8. Conclusions

A wind-tunnel aerofoil test rig has been designed and built, making use of a single control surface operated by a 'V' stack piezo-actuator. Eigenvalues have been assigned successfully and control of flutter has been demonstrated using the receptance method and the flutter-margin prediction procedure. In the experiments carried out with this particular aerofoil system the flutter speed was increased by around 15 % when pole placement was applied to separate the heave and pitch frequencies. Pole placement to increase the damping, principally of the pitch mode, was found to less effective than separating the heave and pitch frequencies in increasing the flutter speed. Further work is now needed to fully establish the extent to which the flutter speed can be increased in the present rig set-up.

Acknowledgement

The authors wish to acknowledge the contributions of Drs Evangelos Papatheou, Simon James and Marco Parandina, and Messrs Steven Bode, Derek Neary and Xiaojun Wei of Liverpool University, Dr Maryam Ghandchi Tehrani of Southampton University and Dr Kumar Vikram Singh of Miami University, Oxford, Ohio.

References

1. H. Zimmerman, Aeroservoelasticity, *Computer Methods in Applied Mechanics and Engineering*, 90(13), 1991, 719-735
2. L. Librescu, Advances in Linear / Nonlinear Control of Aeroelastic Structural Systems, *Acta Mechanica*, 178, 2005, 147-186.
3. J.R. Wright & J.E. Cooper, Introduction to Aircraft Aeroelasticity and Loads, 2007, John Wiley.
4. Fung, Y., 1995, An *Introduction to the Theory of Aeroelasticity*, Dover (original 1955).
5. Hodges, D.H. and Pierce, G.A., 2002, *Introduction to Structural Dynamics and Aeroelasticity*, Cambridge University Press, 2002.
6. De Marqui, C. Jr., Belo, E. M., Marques, F. D., 2004, Wind-Tunnel Model and a Controller for Flutter Suppression, *45th AIAA/ASME/ASCE/AHS/ASC Structures, Structural Dynamics & Materials Conference*, 19-22 April 2004, Palm Springs, California, AIAA 2004-1854.
7. Njuguna, J., 2007, Flutter prediction, suppression and control in aircraft composite wings as a design prerequisite: A survey, *Structural Control and Health Monitoring*, 14, pp. 715–758.
8. Buttrill, Carey S., Bacon, Barton J., Heeg, Jennifer, and Houck, Jacob A., 1996, *Aeroservoelastic Simulation of an Active Flexible Wing Wind Tunnel Model*, NASA Technical Paper 3510.
9. Mottershead, J. E. and Ram, Y. M., Inverse eigenvalue problems in vibration absorption: passive modification and active control, *Mechanical Systems and Signal Processing,* 20(1), 2006, 5-44.
10. Ram, Y.M. and Mottershead, J.E., 2007, Receptance method in active vibration control, *American Institute of Aeronautics and Astronautics Journal*, 45(3), pp. 562-567.
11. Mottershead, J.E., Tehrani, M.G., James, S. and Ram, Y.M., 2008, Active vibration suppression by pole-zero placement using measured receptances, *Journal of Sound and Vibration,* 311(3-5), pp. 1391-1408.
12. Mottershead, J.E., Tehrani, M.G. and Ram, Y.M., 2009, Assignment of eigenvalue sensitivities from receptance measurements, *Mechanical Systems and Signal Processing*, 23(6), pp.1931-1939.
13. Ram, Y.M., Singh, A. and Mottershead, J.E., 2009, State feedback with time delay, *Mechanical Systems and Signal Processing*, 23(6), pp. 1940-1945.
14. Tehrani, M. G., Mottershead, J. E., Shenton, A. T., and Ram, Y. M., 2010, Robust pole placement in structures by the method of receptances, *Mechanical Systems and Signal Processing*, doi:10.1016/j.ymssp.2010.04.005.
15. Tisseur, F., and Meerbergen, K., The Quadratic Eigenvalue Problem, *SIAM Review*, Vol. 43, No. 2, 2001, pp. 235–286.
16. Karpel, M., 1990, Time Domain Aeroservoelastic Modeling Using Weighted Unsteady Aerodynamic Forces, *Journal of Guidance, Control, and Dynamics*, Vol. 13, No. 1, pp. 30–37.
17. Bendat, J. S. and Piersol, A. G., *Random Data: Analysis & Measurement Procedures, Third Edition*, John Wiley and Sons, New York, 2000.
18. Peeters, B., Lowet, G., Van der Auweraer, H., and Leuridan, J., A new procedure for modal parameter estimation, *Journal of Sound and Vibration*, 38(1), pp. 24-29, 2004.
19. Tehrani, M. G., Elliott, R.N.R., and Mottershead, J.E., 2010, Partial pole placement in structures by the method of receptances: theory and experiments, *Journal of Sound and Vibration*, 329 (24), pp. 5017-5035.

20. Ardelean, E.V. and Clark R.L., V-Stack Piezoelectric Actuator, *SPIE Smart Structures and Materials*, 4333, 2001, 322–333.
21. Ardelean, E.V., McEver, M.A., Cole D.G. and Clark R.L., Active flutter control with V-stack piezoelectric flap actuator*, AIAA Journal of Aircraft*, 43(2), 2006, 482-486.
22. Zimmerman, N.H. and Weissenburger, J.T., Prediction of flutter onset speed based on flight testing at subcritical speeds, *AIAA Journal of Aircraft*, 1(4), 190-202, 1964.
23. Price, S.J. and Lee, B.H.K., Evaluation and extenstion of the flutter-margin method for flight flutter prediction, *AIAA Journal of Aircraft,* 30(3), 395-402, 1993.
24. Dimitriadis. G. and Cooper, J.E., Flutter prediction from flight flutter test data, *AIAA Journal of Aircraft,* 38(2), 355-367, 2001.